Michaelides, O., Gazetas, G., Bouckovalas, G. & Chrysikou, E. (1997). *Géotechnique* **48**, No. 1, 33–53

Approximate non-linear dynamic axial response of piles

O. MICHAELIDES,* G. GAZETAS,* G. BOUCKOVALAS* and E. CHRYSIKOU*†

The axial dynamic response of a single pile in clay is examined within the framework of a Winkler-type approach. Experimental data for the variation of soil shear modulus and hysteretic damping with the amplitude of shear strain and the soil 'plasticity' index are curve-fitted and utilized in simulating in a realistic way the non-linearity of the surrounding soil arising from the stresses induced by the pile. An equivalent radially-inhomogeneous but linearly-hysteretic continuum is established, and the 'springs' and 'dashpots' of the dynamic Winkler model are obtained at each depth by solving analytically the pertinent plane-strain (in *z*) and axisymmetric (in *r*) elastodynamic problem. Slippage at the pile–soil interface is also taken into consideration in a simple approximate way. Analytical results are presented to demonstrate the practical significance of soil non-linearity, soil 'plasticity' index and interface slippage in the dynamic stiffness and damping of the pile.

KEYWORDS: dynamics; numerical modelling and analysis; piles; soil/structure interaction; stiffness; vibration.

Les auteurs examinent la réaction dynamique axiale d'un pieu dans l'argile dans le contexte d'une approche du type Winkler. Après l'ajustement de courbe, les données expérimentales obtenues pour la variation du module de cisaillement et de l'amortissement hystérétique en fonction de la déformation de cisaillement et de l'indice de «plasticité» du sol sont utilisées pour simuler de façon réaliste la non-linéarité du sol environnant sous l'effet des tensions engendrées par le pieu. Un continuum équivalent, non homogène radialement, mais hystérétique linéairement, est établi, et les «ressorts» et «amortisseurs» du modèle dynamique de Winkler sont obtenus à chaque profondeur par résolution analytique du problème élastodynamique de la déformation plane (en *z*) et axisymétrique (en *r*). On tient également compte, de façon approximative et simple, du glissement à l'interface pieu-sol. Les résultats de l'analyse sont présentés pour démontrer les effets pratiques de la non-linéarité du sol, de l'indice de plasticité du sol et du glissement interfacial sur la rigidité dynamique et l'amortissement du pieu.

INTRODUCTION

A widely used method for evaluating the dynamic axial response of piles replaces the soil surrounding the pile with a series of independent springs and dashpots (Winkler approach). This implies that shear waves, emitted from the pile periphery, propagate only horizontally and plane-strain conditions prevail. Radial soil displacements are neglected. Soil, therefore, deforms solely in pure shear—an assumption also used with success for statically-loaded piles (Randolph & Wroth, 1978; Baguelin & Frank, 1979), and for the dynamic interaction of piles in a group (Dobry & Gazetas, 1988).

The frequency-dependent moduli of the (continuously distributed along the pile length) Winkler springs and dashpots are obtained by solving the elastodynamic problem of a unit-thickness soil layer of infinite lateral extent, containing an oscillating rigid inclusion (the pile slice). Most solutions are based on the additional simplifying assumption that the soil is radially homogeneous. This, however, may not be realistic even with horizontally uniform soils, because the effective (secant) modulus of the soil in the vicinity of the pile will be reduced to lower than the free-field values, owing to the comparatively large amplitudes of the induced shear strains and the ensuing non-linear soil response.

Novak & Sheta (1980) were the first to propose the use of a massless, narrow, annular boundary zone around the pile, having a shear modulus G_{in} smaller than the modulus G_s of the outer surrounding zone (i.e. of the free field), and larger material damping. The purpose of such a 'soft' zone was to account in an approximate way for both soil non-linearity in the region of highest stresses and slippage (and other 'deficiencies') at the pile–soil interface (Novak, 1991; Pender, 1993). Neglecting the mass of the boundary zone was necessary in order to prevent wave reflections from the fictitious

Manuscript received 17 November 1995; revised manuscript accepted 11 September 1996.
Discussion on this paper closes 1 May 1998; for further details see p. ii.
* National Technical University, Athens.
† Massachusetts Institute of Technology.

discontinuity at the interface between the cylindrical zone and the outer region. On the other hand, the solution, by Veletsos & Dotson (1986), included the inertia of the boundary zone; hence the resulting stiffness and damping exhibited undulations with frequency. More appropriate continuous (monotonically increasing) variations of modulus with radial distance, $G = G(r)$, assumed by Gazetas & Dobry (1984a) and Veletsos & Dotson (1988), eliminated the problem of the spurious wave reflections at the interface between 'boundary zone' and the surrounding soil.

The previous contributions address the problem of lateral soil heterogeneity with only qualitative reference to the non-linear soil response, since the variations of soil properties employed are merely hypothetical. To aid practical applications, this paper utilizes experimental data (e.g. Vucetic & Dobry, 1991) on the dependence of the secant shear modulus and hysteretic damping of soil on the shear strain amplitude and the nature of the soil (the latter represented by the plasticity index I_P). The variation of modulus and damping is then related to the magnitude of the applied load through the amplitude of the induced strains. Thus, the radial inhomogeneity studied models the non-linearity of soil in shear realistically (although approximately). In addition, slippage at the pile–soil interface is also modelled in a simple, realistic way.

PROBLEM DEFINITION AND OUTLINE OF METHOD

The problem studied is that of a floating cylindrical pile embedded in a layered soil deposit and subjected to harmonic axial load at the top (Fig. 1). Initially, before applying any static or dynamic load, all soil layers are assumed to be laterally homogeneous (Fig. 1(a)), implying that any installation effects have 'dissipated'. Applying the static load, shear stresses τ_0 develop on the elements of each layer. To a good approximation, τ_0 is inversely proportional to the radial distance from the pile (Randolph & Wroth, 1978).* A dynamic load $P_c \cos \omega t$ generates additional stresses $\pm\tau_c \cos(\omega t + \theta)$ on the soil elements (Fig. 2), where τ_c is the amplitude of the stresses and θ is the phase difference with respect to the applied

* Notice, however, the slightly different notation in this paper.

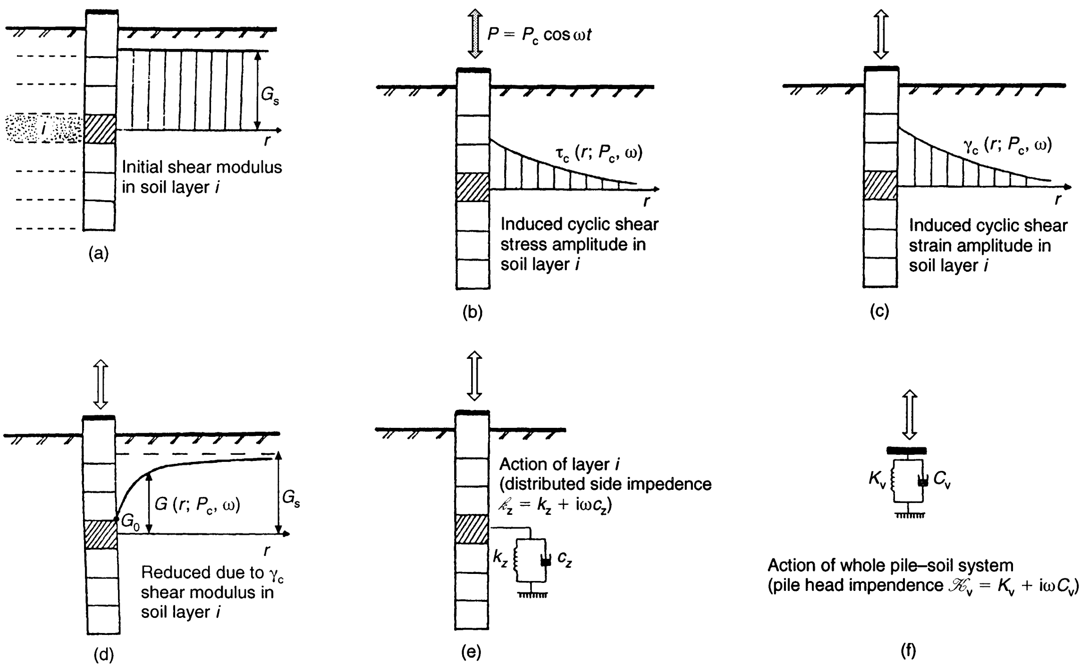

Fig. 1. Steps of the methodology developed in this paper and definition of the impedances $\mathscr{k}_z$ and $\mathscr{K}_v$: (a) initial, radially uniform distribution of shear modulus $G = G_s$ for each horizontal layer; (b) and (c) attenuation with increasing radial distance of the shear stress and shear strain amplitudes induced by load $P_c \cos \omega t$; (d) strain-compatible ('effective') shear modulus $G = G(r; P_c, \omega)$; (e) generalized Winkler-type reaction of each soil layer as represented with a 'spring' (k_z) and a 'dashpot' (c_z), both functions of P_c and ω; (f) complete pile–soil system represented with both K_v and C_v dependent on load-amplitude and frequency

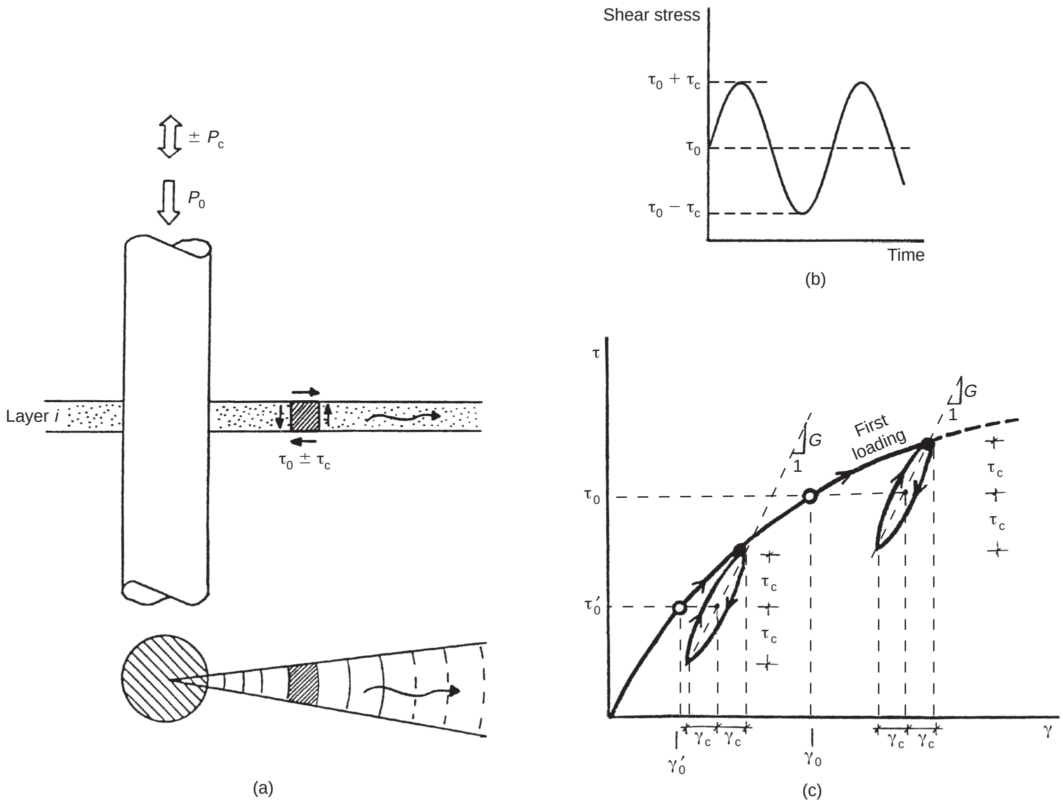

Fig. 2. (a) The fundamental approximation: shear waves from the shaft periphery propagate horizontally under plane strain conditions; (b) variation of shear stress with time in cycling loading; (c) stress–strain behaviour of a soil element under initial shear stress τ_0 and a sinusoidal imposed cyclic shear stress of amplitude τ_c; the hysteresis loops developing after completion of the first loading are essentially identical for two different initial shear stresses τ_0 and τ_0'

load. Figs 1(b) and 1(c) schematically illustrate the radial distribution of the amplitudes of cyclic shear stress τ_c and cyclic shear strain γ_c. They both depend, for a given soil and pile, on the amplitude of the applied load (P_c) and the frequency of excitation (ω).

The radial variation of shear strain greatly affects the value of the secant ('effective') shear modulus and the generated hysteretic damping of the surrounding soil—with the modulus decreasing and the damping increasing in the vicinity of the pile. The soil now becomes, 'effectively', radially inhomogeneous (Fig. 1(d)). Experimental data for clays are utilized in estimating the degree of this 'effective' inhomogeneity, and the elastodynamic problem of the axisymmetric radially-inhomogeneous unbounded soil layer containing a vibrating inclusion (the pile slice) is solved analytically. The reaction of each soil layer is then represented with a (frequency-dependent) 'spring' and 'dashpot', k_z and c_z, as in Fig. 1(e). Finally, the *total* pile head stiffness and damping K_v and C_v (Fig. 1(f)) are obtained from the solution of the differential equation of motion of the (axially deformable) pile continuously supported by the Winkler-type axial 'springs' and 'dashpots' of Fig. 1(e). The effect of slippage between the soil and the pile is also examined in the paper, in an approximate way (however, this is not shown in the figure).

DYNAMIC SHEAR STRESS DISTRIBUTION

In principle, the cyclic stress–strain response of the soil depends on both the static (initial) and the cyclic (induced) shear stresses. For low, moderate and moderately high intensities of cyclic loading, however, one may overlook the effect of static shear stresses and focus solely on the effect of cyclic shear stresses or strains. This argument is suggested by the well known Masing (1926) criterion for unloading–reloading of soils, illustrated in Fig. 2. Only for the first loading from τ_0 to $\tau_0 + \tau_c$ does the resulting strain depend on τ_0; thereafter the loops depend solely on the size of τ_c (or γ_c).

This is also substantiated by experimental evidence. For instance, Fig. 3 shows typical results from cyclic direct simple shear tests on a clay (Andersen, 1992), which clearly demonstrate that the cyclic shear strain amplitude γ_c (and thereby the corresponding secant shear modulus $G = \tau_c/\gamma_c$) at different stages of cyclic loading remain practically constant for the entire possible range of static shear stresses τ_0 and shear strains γ_0, at least for the numbers of loading cycles of interest in earthquake engineering.

Evidently, the radial distributions of τ_c, γ_c and G, sketched in Figs 1(b), 1(c) and 1(d), are interdependent. For example, the distributions $\tau_c = \tau_c(r)$ and $\gamma_c = \gamma_c(r)$ cannot be computed until the soil modulus $G = G(r)$ is already known; $G(r)$, however, is obtained from soil data only after the distribution of strains $\gamma_c(r)$ is known.

Strictly speaking, the problem of determining τ_c (or γ_c) and G can be solved only with an iterative procedure. Fortunately, however, the radial distribution of shear stresses $\tau_c(r)$ turns out to be quite insensitive to variations in the radial distribution of shear modulus $G(r)$. This insensitivity is demonstrated in Appendix 1, where the elastic stress distributions $\tau_c(r)$ for a (radially) homogeneous and two radially inhomogeneous soil layers, computed analytically (and rigorously), are shown to be quite similar for most frequencies of practical significance.*

This observation simplifies considerably the implementation of the method of Fig. 1. The induced shear stresses are obtained, *a priori*, for a homogeneous soil (i.e. without knowing the exact variation of $G(r)$). As shown in Appendix 1,

$$\tau_c(r) = \tau_{c0}\sqrt{\left(\frac{J_1^2\left(a_0\dfrac{r}{R}\right) + Y_1^2\left(a_0\dfrac{r}{R}\right)}{J_1^2(a_0) + Y_1^2(a_0)}\right)} \tag{1a}$$

in which R is the pile radius, $\tau_{c0} = \tau_c(R)$ is the amplitude of the imposed cyclic shear stress at the pile–soil interface,

$$a_0 = \omega R / V_{s0} \tag{1b}$$

$V_{s0} = V_s(R)$ is the S-wave velocity at $r = R$, J_1 and Y_1 are the first-order Bessel functions of the first and second kind respectively, and ω is the circular frequency of the applied force.

Equation (1) can be simplified to

$$\tau_c(r) = \tau_{c0}\frac{R}{r}F(a_r) \tag{2a}$$

where

$$F(a_r) \approx 1 \text{ if } a_r < 1$$
$$F(a_r) \approx {a_r}^{0.57} \text{ if } a_r > 1 \tag{2b}$$

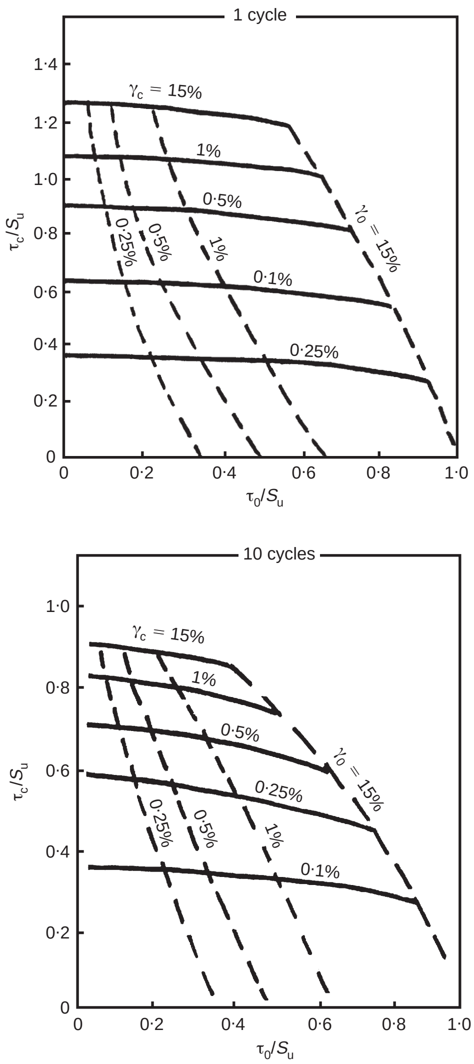

Fig. 3. Static and cyclic shear stresses and resulting strains in simple shear test on Drammen clay with OCR = 1 (from Andersen, 1992); the solid curves are nearly horizontal, implying insensitivity of cyclic response to initial shear stress τ_0

* This finding is reminiscent of the (then) astonishing finding about 25 years ago by Gibson (1967, 1968, 1974) that the stresses in a half-space with G proportional to depth and $\nu = \frac{1}{2}$ are identical to those in a homogeneous half-space. This result was surprising because, in the words of Gibson, 'it paid no regard to the well-known doctrine that more rigid material attracts stress'. (See also Gibson & Sills (1972)).

in which

$$a_r = \omega r / V_s(r) \quad (2c)$$

(Morse & Ingard, 1968; Bouckovalas *et al.*, 1992).

Notice that for ω approaching 0 (static case), equation (2) reduces to the aforementioned 'cylindrical' solution of Randolph & Wroth (1978) and Baguelin & Frank (1979).

RADIAL VARIATION OF MODULUS AND DAMPING: EXPERIMENTAL DATA AND MODELLING

The variation with shear strain amplitude of the shear modulus $G = G(\gamma)$ and the hysteretic damping $\xi = \xi(\gamma)$ has been studied experimentally by numerous investigators in both cyclic (Seed & Idriss, 1970; Richart & Wylie, 1977; Dobry & Vucetic, 1987) and monotonic (Jardine *et al.*, 1984; Burland, 1989) experiments. Vucetic & Dobry (1991) synthesized a variety of experimental data and proposed the dashed curves plotted in Fig. 4, where G_s is the shear modulus at low strain levels ($\gamma < 10^{-5}$) and I_P is the plasticity index of the soil (in %).

The effect of the so-called 'plasticity'* index I_P seems to be substantial. As I_P increases, the ratio $G(\gamma)/G_s$ increases and ξ decreases. This indicates that the soil behaviour remains essentially elastic for increasingly larger values of shear strain as I_P increases.

The following equation was fitted to the data of Fig. 4 (Chrysikou, 1993):

$$\frac{G(\gamma)}{G_s} = 1 - \left\{ \left(2700 \gamma_c \frac{G}{G_s} \right)^{0.72} 10^{-(I_P/\lambda)} \right\} \quad (3)$$

or, in terms of the shear stress amplitude $\tau_c(r)$,

$$\frac{G(\gamma)}{G_s} = 1 - \left\{ \left(2700 \frac{\tau_{c0}}{G_s} \frac{\tau_c(r)}{\tau_{c0}} \right)^{0.72} 10^{-(I_P/\lambda)} \right\} \quad (4)$$

in which λ is a function of the 'plasticity' index:

$$\lambda \approx 0.002(I_P)^2 + 0.25(I_P) + 60 \quad (5)$$

The experimental curves of the variation of hysteretic damping with shear strain are described by the following set of expressions:

$$\xi = 2 + [18 - 0.08(I_P - 15)](1 - G/G_s) \quad \text{if } 0 \leqslant I_P < 100$$

$$\xi = 2 + 11.2(1 - G/G_s) \quad \text{if} \quad I_P \geqslant 100 \quad (6)$$

The good agreement between the proposed expressions and the experimental data is evident in Fig. 4.

* The quotation marks around the word 'plasticity' are to remind one that increasing I_p increases the *elasticity* (not the plasticity) of a clay.

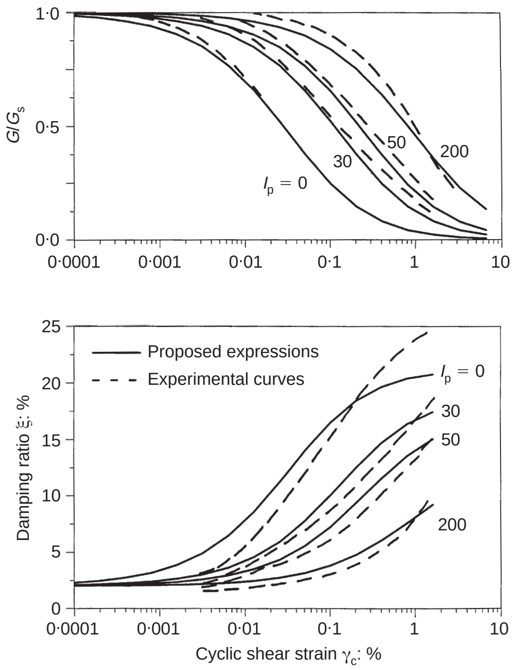

Fig. 4. Comparison of proposed expressions for shear-strain dependence of secant shear modulus and hysteretic damping ratio (equations (3) and (6)) with experimental design curves proposed by Vucetic & Dobry (1991)

Inserting equation (2) for the radial distribution of the dynamic shear stress amplitude into equation (4), a radial variation of the shear modulus is obtained:

$$\frac{G(r)}{G_s} = 1 - \left\{ \left[2700 \frac{\tau_{c0}}{G_s} 10^{-1.4(I_P/\lambda)} \right] \times \left[\frac{R}{r} F(a_r) \right] \right\}^{0.72} \quad (7)$$

or, alternatively,

$$\frac{G(r)}{G_s} = 1 - \left\{ \Lambda \frac{R}{r} F(a_r) \right\}^{0.72} \quad (8)$$

where Λ, hereafter called the 'loading intensity factor', is

$$\Lambda = 2700 \frac{\tau_{c0}}{G_s} 10^{-(1.4 I_P/\lambda)} = 2700 \frac{\tau_{c0}}{f_s} \frac{10^{-1.4(I_P/\lambda)}}{G_s/\alpha S_u} \quad (9)$$

where $f_s = \alpha S_u$ is the frictional capacity of the soil–pile interface, with S_u being the undrained shear strength of the soil and α the well-known reduction factor, deduced empirically from pile load tests, in function of the S_u/σ'_{v0} ratio and the slenderness L/R of the pile (Poulos & Davis, 1980; Fleming *et al.*, 1985; Tomlinson, 1986; Poulos, 1988). Typical values of α for usual pile lengths are

$\alpha = 1$	for soft clays
$1 > \alpha > 0{\cdot}4$	for stiff clays
$\alpha \approx 0{\cdot}4$	for hard clays.

It is presently well established that the shear modulus of a clay can be expressed as a multiple of the undrained shear strength, in the form $G_s = \eta S_u$ where typically the coefficient η ranges around 1000. Recent experimental data show that η is also affected by the 'plasticity' index. For instance, Larsson & Mulabdic (1991) give the following expression for clays with medium to high values of the 'plasticity' index:*

$$\frac{G_s}{S_u} \approx \frac{20\,000}{I_P} + 250 \tag{10}$$

Equations (9) and (10) reveal that the loading intensity factor Λ is primarily a function of the ratio of the induced cyclic shear stress amplitude to the 'frictional' capacity of the interface, while it also encompasses the effect of the soil 'plasticity' index.

Figure 5 shows typical diagrams, obtained from equation (8), for the radial variation of shear modulus and hysteretic damping ratio, computed for different values of the loading intensity factor Λ and different frequency factors $a_0 = \omega R / V_{s0}$. It is observed that the shear modulus and the hysteretic damping ratio of the soil change most rapidly in the immediate vicinity of the pile, while at larger radial distances they tend asymptotically to the corresponding free-field values.

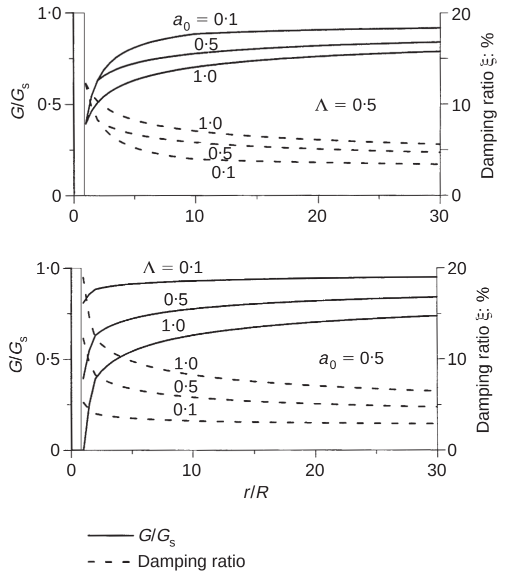

Fig. 5. Radial distribution of effective shear modulus $G = G(r)$, reflecting the fact that shear strain amplitudes decrease with radial distance from the pile

DYNAMIC SOIL REACTION ('SPRING' AND 'DASHPOT' FOR A PILE SLICE)

No slippage at the pile–soil interface

The governing differential equation of motion for the vertically excited inhomogeneous layer of unit thickness is derived from the dynamic equilibrium of shear and inertial forces in an elemental soil ring (Dotson & Veletsos, 1990; Gazetas & Dobry, 1984a; Novak, 1974; Novak *et al.*, 1978; Veletsos & Dotson, 1988):

$$G\frac{d^2 w}{dr^2} + \left(\frac{dG}{dr} + \frac{G}{r}\right)\frac{dw}{dr} = \rho\frac{\partial^2 w}{\partial t^2} \tag{11}$$

A closed-form analytical solution to this equation cannot be obtained if $G(r)$ is described with equation (8). Moreover, efforts to simplify equation (8) so that equation (11) could be solved analytically were not successful (Michaelides & Gazetas, 1995). By contrast, solutions *have* been presented for the static problem (Kraft *et al.*, 1981; Kuwabara, 1991). To overcome this difficulty, the soil was divided into four inhomogeneous† ring zones and the 'exact' radial variation of shear modulus (as given in equation (8)) was numerically curve-fitted with the following exponential expressions:

$$G(r) = G_0{}^*\left(\frac{r}{R}\right)^{m_0} \quad \text{for } r < R_1$$

$$G(r) = G_1{}^*\left(\frac{r}{R_1}\right)^{m_1} \quad \text{for } R_1 < r < R_2$$

$$G(r) = G_2{}^*\left(\frac{r}{R_2}\right)^{m_2} \quad \text{for } R_2 < r < R_3$$

$$G(r) = G_3{}^* \quad \text{for } r > R_3 \tag{12}$$

in which

$$G_j{}^* = G_j(1 + i2\xi_j), \quad j = 0, 1, 2, 3$$

* As this article was being finalized, a paper was published by Viggiani & Atkinson (1995) containing a wealth of experimental data, relating shear modulus at small strain levels to the mean effective stress, in the form $G_s = A(\sigma'_v)^n$. For the experimental parameter A, a function of the plasticity index, we curve-fitted the expression $A \approx 25\,000/I_p$ to their data. The similarity to equation (10) is apparent.

† Although a discretization of the soil medium into a number of *homogeneous* ring elements could in principle also be used, the large gradient of $G(r)$ in the vicinity of the pile would lead to spurious wave reflections due to the unavoidable sharp discontinuity in G across the interface of two zones.

and G_j are the moduli at the boundaries of each zone, given by

$$G_1 = G_0\left(\frac{R_1}{R}\right)^{m_0}$$
$$G_2 = G_1\left(\frac{R_2}{R_1}\right)^{m_1}$$
$$G_3 = G_2\left(\frac{R_3}{R_2}\right)^{m_2}$$

where $\mathrm{i} = \sqrt{(-1)}$; G_0 is the shear modulus at the pile–soil interface; ξ_0, ξ_1, ξ_2 and ξ_3 are the material hysteretic damping at the beginning of each zone (obtained using equations (6) and (8)); and R_1, R_2 and R_3 (radii of the zones) and m_0, m_1 and m_2 are functions of the dimensionless frequency $a_s = \omega R/V_s$ (V_s being the far-field S-wave velocity) and the loading intensity factor Λ (see equation (9)). These parameters (R_j, m_j) were obtained by numerically curve-fitting the data of Fig. 5.

By using the power variation of $G(r)$ given in equation (12), the differential equation of motion for harmonic excitation

$$w(r,\ t) = w(r)\,\mathrm{e}^{\mathrm{i}\omega t} \tag{13}$$

becomes

$$\zeta^2 \frac{\mathrm{d}^2 w}{\mathrm{d}\zeta^2} + (m_j + 1)\zeta\frac{\mathrm{d}w}{\mathrm{d}\zeta} + \lambda_j{}^2\zeta^{2-m_j}w = 0, \qquad j = 0,\ 1,\ 2 \tag{14}$$

where

$$\lambda_j = a_j/(1 + 2\mathrm{i}\xi), \quad a_j = \frac{\omega R}{V_s(r)}, \quad j = 0,\ 1,\ 2$$
$$a_0 = \frac{\omega R}{V_s(R)}, \quad m_j = m_0, \quad \text{for } r < R_1$$
$$a_j = a_{j-1}\left(\frac{R_j}{R}\right)^{(m_j - m_{j-1})/2},$$
$$\text{for } R_j < r < R_{j+1} \quad \zeta = r/R, \quad \text{for all zones.} \tag{15}$$

Equation (14) is a generalized Bessel differential equation, the solution of which is

$$w = \zeta^{-m/2}[A_i H^{(1)}_{\kappa-1}(\kappa\lambda_0\zeta^{1/\kappa}) + B_i H^{(2)}_{\kappa-1}(\kappa\lambda_0\zeta^{1/\kappa})] \tag{16}$$

where

$$\kappa = \frac{2}{2 - m_j}$$

and $H^{(\ )}_{\kappa}$ is the κ-order Hankel function of the first or second kind respectively (Abramowitz & Stegun, 1972; Spiegel, 1971).

The boundary conditions are a (known) displacement $\delta_c\,\mathrm{e}^{\mathrm{i}\omega t}$ is imposed at the pile–soil interface, displacements vanish as $\zeta \to \infty$ and displacements and stresses are continuous at the interfaces of the four ring zones. Enforcing these boundary conditions leads to a system of algebraic equations, from which the eight complex-valued constants A_i and B_i are determined. The complex dynamic stiffness of the pile–soil system is then obtained:

$$\begin{aligned}\mathscr{k}_z &= -2\pi G_0{}^*\left(\frac{\mathrm{d}w}{\mathrm{d}\xi}\right)_{\zeta=1} \\ &= 2\pi G_0{}^*\lambda_0[A_0 H^{(1)}_{\kappa}(\kappa\lambda_0) + B_0 H^{(2)}_{\kappa}(\kappa\lambda_0)]\end{aligned} \tag{17}$$

Equation (17) can be expressed in two alternative forms

$$\mathscr{k}_z = k_{\mathrm{real}} + \mathrm{i}k_{\mathrm{imag}} = k_z + \mathrm{i}\omega c_z \tag{18}$$

where $k_z = k_{\mathrm{real}}$ and $c_z = k_{\mathrm{imag}}/\omega$ are the (frequency-dependent) moduli of the 'spring' and 'dashpot' that model the soil reaction against the oscillating pile slice; k_z reflects the stiffness and (distributed) inertia of the surrounding soil, while c_z represents the radiation of wave energy away from the pile plus the energy dissipated in hysteretic action in the soil (e.g. Gazetas, 1983; Gazetas & Dobry, 1984b).

Results of the analysis are presented in Figs 6–8. Fig. 6 portrays in dimensionless form the variation with frequency of the spring and dashpot moduli, for different values of the load intensity factor Λ. Recall that G_s and V_s are the shear modulus and shear wave velocity at low strain levels, that is, in the far field ($r \to \infty$). To visualize better the importance of soil non-linearity, the same results are replotted in Fig. 7, but normalized with respect to the corresponding solution for linear soil ($\Lambda = 0$). Finally, Fig. 8 uses the results of Fig. 6 for $\Lambda = 0$ and 0·5 to illustrate the relative contributions of the real and imaginary parts to the overall (complex) stiffness.

The following trends are worthy of note in these figures.

(*a*) As soil non-linearity increases with increasing 'loading intensity factor' Λ, the stiffness k_z of the pile–soil system (the spring modulus), predictably, decreases. The rate of decrease 'accelerates' with frequency ω, especially for high Λ values. As a result, k_z becomes negative (implying a phase difference of 180° between pile force and displacement) when both a_s and Λ are relatively large. Stated in different words, the frequency factor a_s at which k_z crosses the zero axis decreases when the loading factor Λ increases.

To explain this behaviour, recall that k_z can be thought of as proportional to the difference of the (overall) shear resistance of the soil minus the

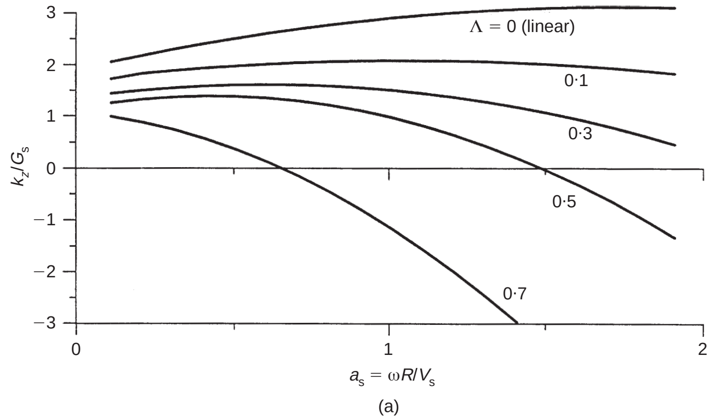

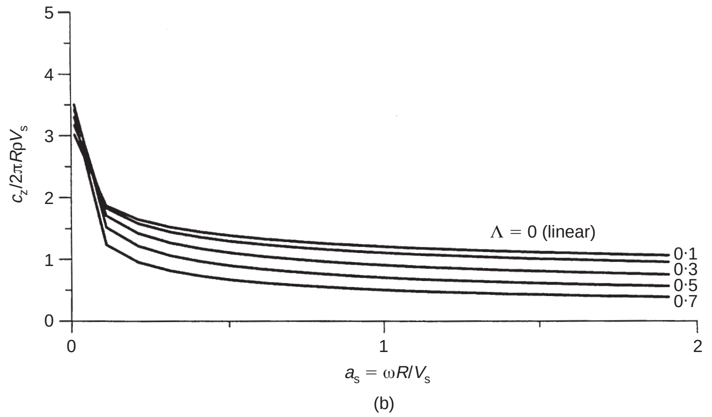

Fig. 6. Results for the dynamic impedance of a pile slice in a horizontal soil layer, showing the effect of dimensionless frequency and level of loading (in terms of Λ); (a) stiffness normalized by the initial (free-field) soil modulus G_s; (b) dashpot modulus normalized by the product ρV_s times the perimeter of the pile

(overall) soil inertia. An increase in frequency leads to increased soil inertia, and thereby to reduced k_z. An increase in load amplitude leads to larger soil non-linearity and reduced soil shear stiffness; thus k_z would also decrease. The increasing (negative) role of soil inertia at high values of loading amplitude suggests that, effectively, a soil mass next to the pile vibrates almost in phase with the pile.

(*b*) The dashpot modulus c_z encompasses both the *hysteretic* damping in the soil (prevalent at low frequency factors $a_s < 0{\cdot}20$) and the *geometric* damping due to radiation of waves from the pile periphery to infinity (dominant at high frequency factors $a_s \geqslant 0{\cdot}20$). It is evident in Figs 6 and 7 that increasing the amplitude of the load and hence increasing non-linearity leads to a decrease in geometric (radiation) damping and an increase in hysteretic damping. These are hardly surprising observations. As the name implies, soil hysteretic damping increases with increasing hysteresis due to non-linearity. On the other hand, radiation of wave energy is proportional to the S-wave velocity in the soil, and with increasing non-linearity this velocity would decrease in the neighbourhood of the pile. In addition, the laterally inhomogeneous soil wave velocity (e.g. Fig. 1(d)) leads to 'continuous reflections' of the radially propagating waves, thereby further undermining radiation damping. In fact, for a linear soil with the S-wave velocity increasing as a power of the radial distance ($V_s(r) = V_{s0}(r/R)^m$, where V_{s0} is the velocity at the interface $r = R$), Gazetas & Dobry (1984a) have shown that, asymptotically, at high frequencies, the radiation dashpot modulus becomes equal to $2\pi R\rho V_{s0}$. This implies that the

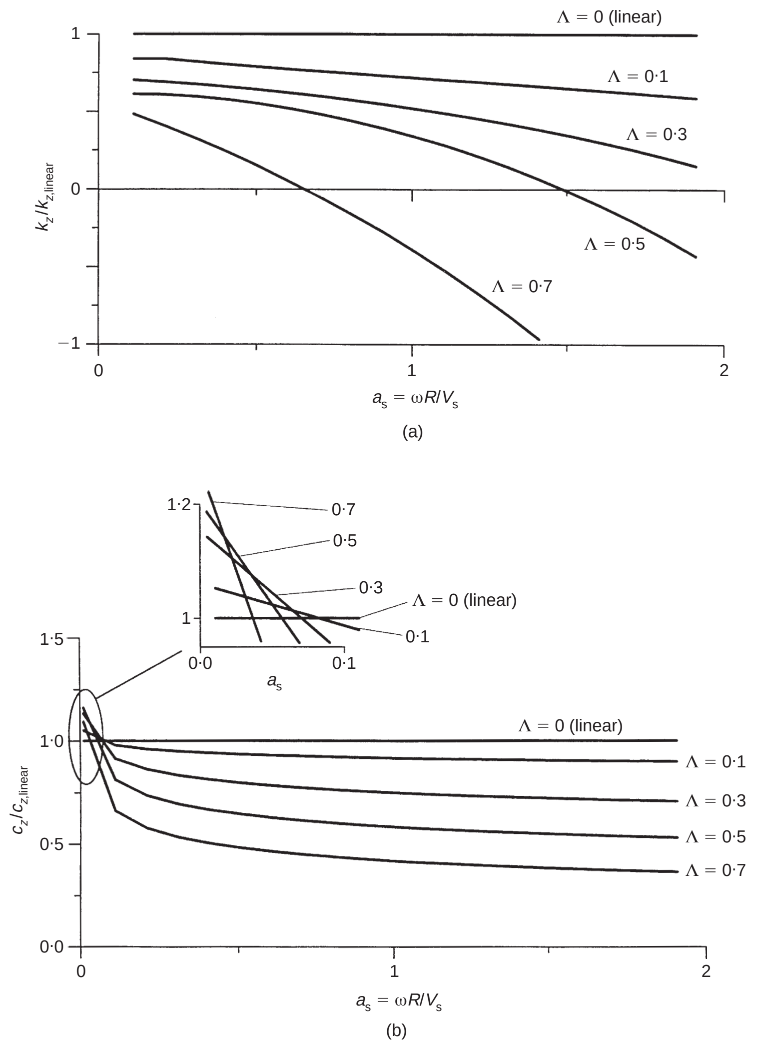

Fig. 7. The results of Fig. 6 for k_z and c_z, normalized by the linear curves $k_{z,\text{linear}}$ and $c_{z,\text{linear}}$

emitted very-high-frequency waves (i.e. waves of vanishingly small wavelength) 'see' the soil surrounding the pile as a homogeneous medium having velocity equal to V_{s0}, that is, the velocity in the immediate vicinity of the source! In Figs 6 and 7 the reader can easily check that the above observation also holds true here, to an excellent degree: the high-frequency value of c_z is proportional to the interface velocity V_{s0}—the latter being a decreasing fraction of the far-field velocity V_s as Λ (and hence soil non-linearity) increases.

(*c*) The imaginary part $k_{\text{imag}} = \omega c_z$ of the complex stiffness (representing the soil reaction that is out of phase with the imposed motion) dominates at all but the very lowest frequency factors.

Slippage at the pile–soil interface

In the previous analysis no slippage occurred between soil and pile. In reality, however, such slippage will take place whenever the total shear stress (static and dynamic) at the interface tends to exceed the frictional capacity ('skin friction') f_s. In that case, the equivalent stiffness of the soil is drastically reduced since, for a given force, the displacement of the pile segment becomes larger.

The detailed effect of slippage on the non-linear stiffness of the pile segment requires rigorous modelling of the cyclic response of the interface and numerical treatment, which are beyond the scope of the very simple solution that is sought in this paper. The aim is to gain a realistic insight

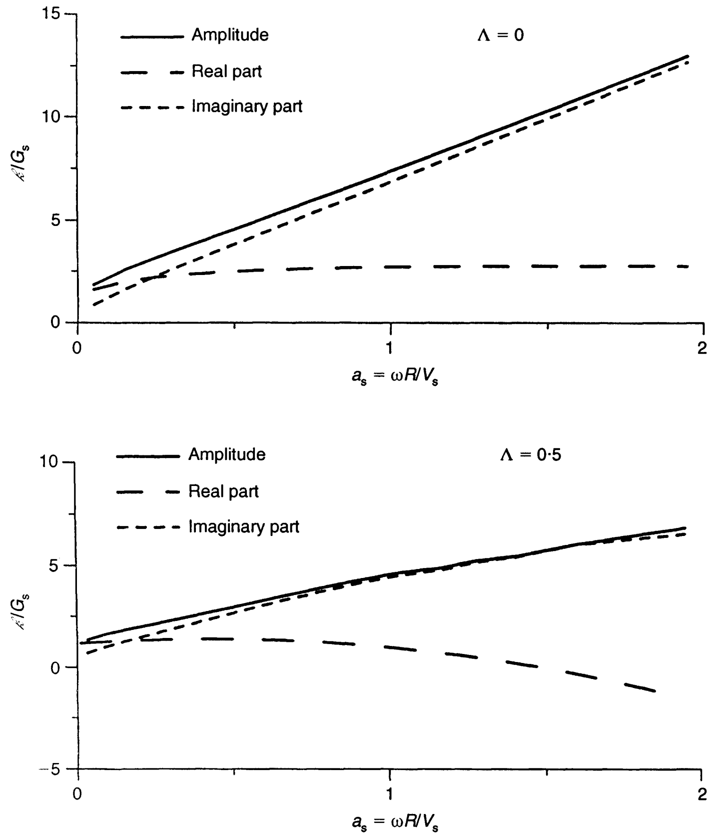

Fig. 8. Comparison of the relative importance of the real ($k_{real} = k_z$) and imaginary ($k_{imag} = \omega c_z$) parts of the amplitude of the dynamic impedance of a pile slice

into the phenomenon and develop an approximate method for estimating its effect relative to the effects of soil non-linearity discussed up to this point. The method is illustrated conceptually in Fig. 9. A pile slice is subjected to an initial static displacement δ_0 (typically of the order of $\frac{1}{2}$ to $\frac{1}{3}$ of the yield displacement δ_s) followed by dynamic loading with constant displacement amplitude $\pm\delta_c$. A mechanical model of soil reaction against such pile motion is depicted in Fig. 9(a). The soil is replaced with a non-linear spring–dashpot element (as in Fig. 1(e)) connected to the pile, *not* directly but through a frictional slider. The non-linear spring–dashpot element is described through a complex-valued impedance $\mathscr{k}_z = k_z + \mathrm{i}\omega c_z$, which is obtained as a function of the amplitude of the interface shear stress τ_{c0} by the method developed in the preceding section and illustrated in the plots of Figs 6–8. The slider is essentially a rigid–plastic element with a yield force $F_s = 2\pi R f_s$. The 'skin friction' f_s is taken here for clayey soils as αS_u (see earlier discussion).

The developed method replaces (at its final stage) the initial ('real') model of Fig. 9(a) with only a single spring–dashpot element, the impedance of which,

$$\mathscr{k}_{zs} = k_{zs} + \mathrm{i}\omega c_{zs} \tag{19}$$

encompasses both soil material non-linearity and pile interface sliding. To make the analysis simpler, the effect of slippage is decomposed into two components, studied separately.

Effect of slippage on the reduction of spring modulus and radiation damping. Figures 9(b), 9(c) and 9(d) explain in a simple manner how the complex modulus $\mathscr{k}_s = k_s + \mathrm{i}\omega c_s$ of a spring–dashpot system is obtained in terms of the possible sliding. To make the picture clear, the initial (i.e. before sliding) force–displacement relationship is replaced with a segment of straight line of slope $\mathscr{k}_z$, that is, the complex equivalent linear modulus before sliding.

With reference to Fig. 9, three possible modes

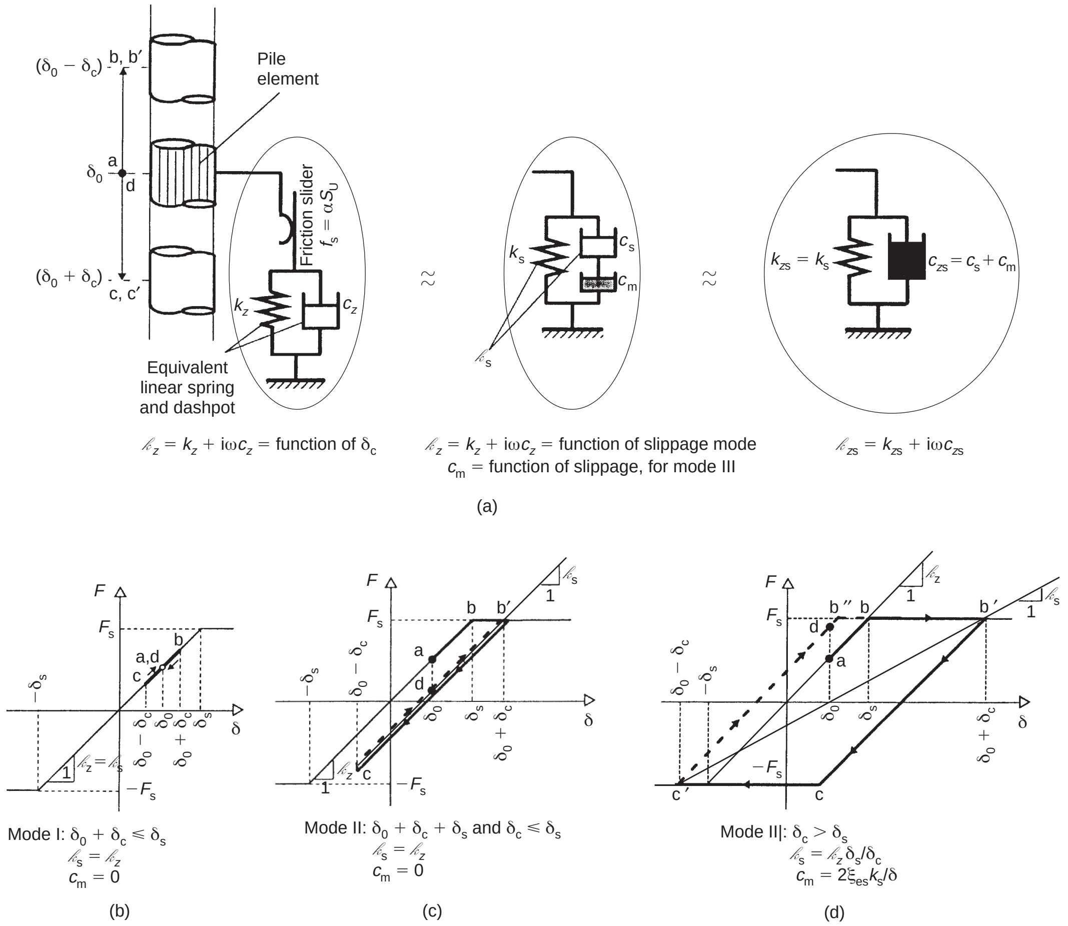

Fig. 9. Load–displacement diagrams (in displacement-controlled vibration of a pile segment) for conceptual illustration of the effect of slippage on pile response: (a) elasto-plastic model of soil reaction against a vibrating pile slice with interface slippage and its equivalent linear approximation; (b), (c) and (d) illustration of the three possible modes with respect to sliding, for the development of the equivalent linear model (all F–δ 'curves' are only shown to be linear for the sake of clarity of the effect of slippage)

of response (in a displacement-controlled vibration) can take place.

Mode I. The maximum displacement $\delta_0 + \delta_c$ remains lower than the displacement δ_s required to initiate slippage of the slider: $\delta_s = F_s/|\mathscr{k}_z|$, that is, the corresponding peak external load $F_0 + F_c$ remains lower than the yield load F_s (Fig. 9(b)). Then, the response of the pile segment is controlled by the stiffness of the surrounding soil, and the equivalent elasto-plastic stiffness $\mathscr{k}_s$ is equal to the equivalent linear stiffness $\mathscr{k}_z$.

Mode II. The maximum displacement $\delta_0 + \delta_c$ becomes larger than the displacement δ_s required to initiate slippage of the slider, but the cyclic displacement amplitude δ_c remains lower than δ_s (Fig. 9(c)). In this case, slippage will occur only on the first-time loading, from δ_0 to $\delta_0 + \delta_c$ (branch abb′ of the loop), while subsequent cycles of unloading and reloading will be sustained by the spring–slider system without further slippage (branch b′cd of the loop). This is achieved by a reduction of the static force on the pile segment that counterbalances the difference between the peak and yield loads during first-time loading. Thus, beyond the very first loading, slippage has essentially no effect on the response of the pile segment. Thus, again, the equivalent elasto-plastic stiffness $\mathscr{k}_s$ is equal to the equivalent linear stiffness $\mathscr{k}_z$.

Mode III. The cyclic displacement amplitude δ_c exceeds the yield displacement δ_s (Fig. 9(d)). In this case, even a reduction of the static load to zero during the first-time loading would not be enough to avoid slippage. Unlike modes I and II, slippage now occurs during all subsequent cycles of loading and unloading, whenever the external load reaches the yield limit (branches b″b′ and cc′ of the loop). As a result, an equivalent elasto-plastic stiffness $\mathscr{k}_s$ can be defined as the slope of the diagonal b′c′ of the loop in Fig. 9(d). Apparently, $\mathscr{k}_s$ is smaller than the equivalent linear stiffness $\mathscr{k}_z$.

On the basis of the geometry of the load–displacement loop in Fig. 9(d), the relative effect of slippage on stiffness may be approximated as

$$\mathscr{k}_s/\mathscr{k}_z \approx \delta_s/\delta_c \tag{20}$$

or, in terms of shear stresses at the pile–soil interface,

$$\mathscr{k}_s/\mathscr{k}_z \approx f_s/\tau_{c0} \tag{21}$$

where f_s is the skin friction and $\tau_{c0} = F_c/2\pi R$ denotes the cyclic shear stress amplitude that would have developed at the pile–soil interface had slippage not occurred.

Effect of slippage on the increase of hysteretic damping. The above 'corrections' for sliding (equation (21)) imply a reduction in both the spring and dashpot moduli ($\mathscr{k}_s = k_s + i\omega c_s$). The decrease of dashpot modulus estimated here stems from the reduction in radiation damping, since no additional waves are emitted from the pile during slippage. On the other hand, slippage dissipates energy. In the conceptual sketch of Fig. 9(d), hysteretic loss of energy takes place during cyclic loading. In fact, the area enclosed by the load–displacement loop increases with the cyclic displacement increment δ_c. An equivalent additional damping ratio (ξ_{es}) can be obtained from the ratio of the area of a complete loop, ΔE_h, to the equivalent elastic energy, $E_{es} = \frac{1}{2}F_s\delta_c$, as follows:

$$\xi_{es} = \frac{\Delta E_h}{4\pi E_{es}} = \frac{2}{\pi}(1 - \delta_s/\delta_c) \tag{22}$$

The additional hysteretic dashpot modulus that must be added to c_s obtained from equation (21) is then approximately given by

$$c_m \approx 2\xi_{es}k_s/\omega \tag{23}$$

This is in addition to the dashpot modulus arising from soil non-linearity, which is hidden in c_z (and c_s). Evidently, when $\delta_c = \delta_s$ this additional equivalent hysteretic damping is zero, while $\mathscr{k}_s = \mathscr{k}_z$, in accordance with the second mode.

Thus the resulting 'total' dashpot modulus c_{zs} either remains equal to c_z (for modes I and II) or is given (for mode III) as the sum of the moduli of the two (in series) dashpots:

$$\begin{aligned} c_{zs} &= c_z \qquad \text{for modes I and II} \\ c_{zs} &= c_s + c_m = c_z f_s/\tau_{c0} \\ &\quad + 2\xi_{es}k_s/\omega \qquad \text{for mode III} \end{aligned} \tag{24a}$$

while the 'total' spring modulus k_{zs} is given by

$$\begin{aligned} k_{zs} &= k_z \qquad \text{for modes I and II} \\ k_{zs} &= k_s = k_z f_s/\tau_{c0} \qquad \text{for mode III} \end{aligned} \tag{24b}$$

The resulting variations of 'spring' and 'dashpot' factors are plotted in Fig. 10 as functions of the cyclic shear stress ratio τ_{c0}/f_s, for a low (near static) and a high (dynamic) value of the dimensionless frequency factor a_s, equal to 0·1 and 1 respectively. The skin friction parameter α is taken equal to 1. As seen in this figure, the effect of slippage on the spring modulus is significant in both of the cases $a_s = 0{\cdot}1$ and 1. On the other hand, for the dashpot modulus slippage is important at high frequencies but practically unimportant at low frequencies. These differences can be attributed to the different relative significance of the aforementioned two counteracting phenomena controlling the dashpot modulus:

(*a*) the increase in hysteretic damping—in inverse proportion to ω according to equation (23)
(*b*) the decrease in radiation damping—nearly independent of ω.

Thus, whereas at low frequencies phenomenon (*a*) is still significant and its effect may overshadow phenomenon (*b*), at high frequencies phenomenon (*a*) becomes insignificant and phenomenon (*b*) dominates. For a simple proof of this explanation, the dashed lines in Fig. 10 represent the dashpot modulus when the additional hysteretic damping (c_m) is ignored. Indeed, at high frequencies (where hysteretic damping is insignificant) this has practically no effect on the dashpot modulus, whereas at low frequencies the effect is substantial, increasing with the amplitude of τ_{c0}/f_s.

DYNAMIC STIFFNESS OF THE WHOLE PILE

The dynamic spring and dashpot moduli obtained for a pile slice in the preceding paragraphs are used in the analysis of a vertically vibrating single pile, in the Winkler-type model sketched in

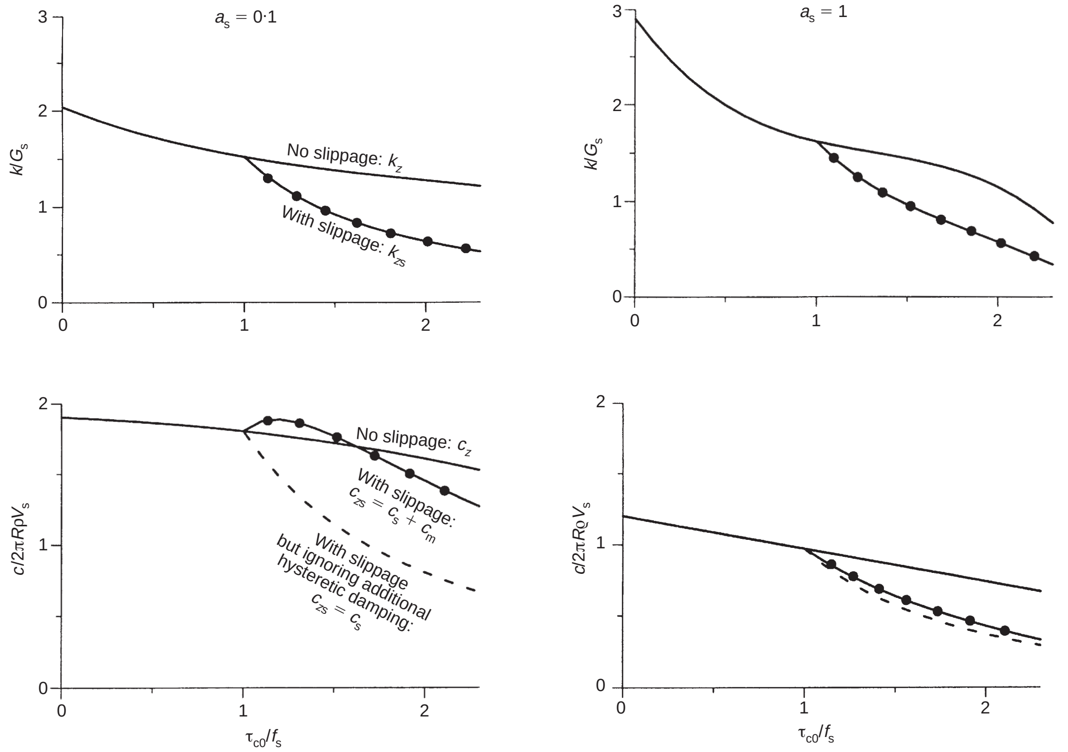

Fig. 10. Effect of slippage on dynamic impedance: the spring modulus k is significantly affected for all frequency values, while the dashpot modulus c is reduced only at high frequencies, where radiation damping dominates; for low frequencies, the presence of the additional hysteretic damping partly counterbalances the reduction of radiation damping due to slippage

Fig. 11. For harmonic steady-state oscillation of the pile,

$$\delta(z,\ t) = \delta_c(z)\,e^{i\omega t} \tag{25}$$

dynamic equilibrium of a pile element yields

$$E_p A_p \frac{d^2\delta_c(z)}{dz^2} - (k_z + i\omega c_z - m\omega^2)\delta_c(z) = 0 \tag{26}$$

where E_p and A_p are the Young's modulus of elasticity and cross-sectional area of the pile, and m is the mass of the pile per unit length. The general solution is

$$\delta_c = A_1\,e^{Dz\cos(\theta/2)}\,e^{iDz\sin(\theta/2)} + A_2\,e^{-Dz\cos(\theta/2)}\,e^{-iDz\sin(\theta/2)} \tag{27a}$$

where

$$D = \left[\frac{(k_z - m\omega^2)^2 + (\omega c_z)^2}{(E_p A_p)^2}\right]^{1/4}$$

$$\theta = \arctan\frac{\omega c_z}{k_z - m\omega^2} \tag{27b}$$

(see e.g. Makris & Gazetas, 1993).

Equation (27) is an implicit relation, since δ_c is given as a function of k_z and c_z, which in turn depend on $\delta_c(z)$. Iterations are therefore needed to derive the solution. It is instructive in this respect to study the following two cases separately.

Flexible piles

For the general case of a flexible pile embedded in layered soil, where shear stresses vary along the pile, an iterative method is followed to account for the effect of soil non-linearity. For each pile slice, the integration constants A_1 and A_2 (equation (27)) are computed by enforcing the continuity of stresses and displacements along the pile axis. Moreover, at the top of the pile

$$\delta(0,\ t) = \delta_c(z = 0)\,e^{i\omega t} \tag{28}$$

while at the pile tip

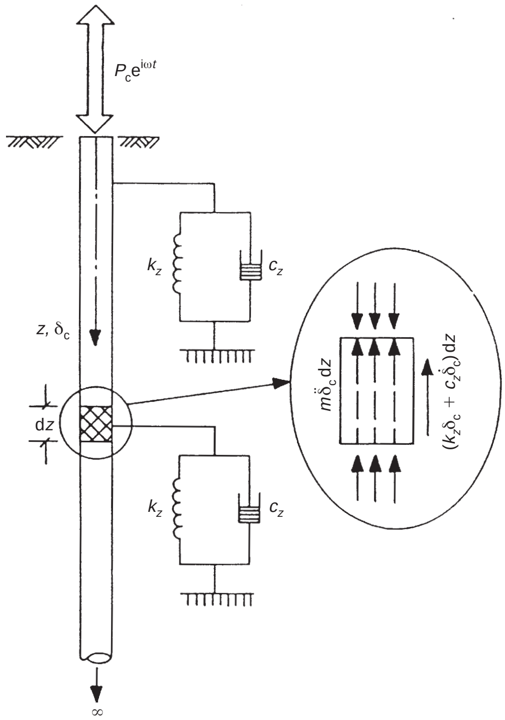

Fig. 11. Winkler model for a vertically vibrating pile (from Makris & Gazetas, 1993)

$$P_b = -E_p A_p \left(\frac{d\delta(z,\, t)}{dz} \right)_{z=L} \tag{29}$$

where P_b is the developing harmonic force at the tip ($z = L$) of the pile. P_b is related to the resulting pile tip displacement $\delta_c(z = L)$ through the dynamic stiffness S_b of the pile base. Accepting the arguments of Randolph & Wroth (1978) and Scott (1981), it is assumed that S_b is approximately equal to the dynamic stiffness of a circular footing on the (underlying) homogeneous half-space:

$$S_b = P_b/\delta_c(z = L) \approx \frac{4G_b R}{1 - \nu_b} + i\omega\pi R^2 \rho_b (V_{La})_b \tag{30}$$

in which G_b, $(V_{La})_b$, ν_b and ρ_b are the shear modulus, 'Lysmer's analogue' wave velocity, Poisson's ratio and the mass density of the soil below the base of the pile. V_{La} is related to the S-wave velocity (Gazetas & Dobry, 1984a,b):

$$V_{La} = \frac{3{\cdot}4}{\pi(1 - \nu)} V_s \tag{31}$$

In the first iteration, the shear stresses along the pile shaft are computed using the *linear* spring and dashpot expressions (Makris & Gazetas, 1993; Makris & Makris, 1991):

$$k_{z,\text{linear}} = 0{\cdot}60 E_s (1 + \tfrac{1}{2}\sqrt{a_s})$$
$$c_{z,\text{linear}} = 1{\cdot}20 a_s^{-1/4} \pi d \rho_s V_s + 2\xi k_z/\omega \tag{32}$$

Then equation (27) gives the complex-valued displacement amplitude $\delta_c(z)$. The shear stress amplitude $\tau_{c0}(z)$ is obtained from

$$\tau_{c0}(z) = \frac{1}{2\pi R} |\mathscr{k}_{z,\text{linear}}(z)\delta_c(z)| \tag{33}$$

where the vertical bars indicate the absolute value of the complex number. The parameter $\Lambda = \Lambda(z)$ is then calculated (equation (9)) and a new set of 'non-linear' springs is obtained, using the proposed method (slippage is taken into account by replacing $\mathscr{k}_z$ with $\mathscr{k}_{zs}$, as described previously). The process is repeated until a reasonable convergence of shear stresses is achieved.

Rigid pile

For the special case of a rigid cylindrical pile and uniform soil properties with depth, a force equilibrium method can be followed. Since the pile is rigid the displacement amplitude is constant along the pile, that is,

$$\delta_c(z = 0) = \delta_c(z = L) = \delta_c(z) = \delta_c \tag{34}$$

The applied force at the head of the pile is equal to the sum of the total force P_s at the pile shaft, the force P_b at the pile tip and the pile inertial force P_{in}. This force equilibrium can be written as:

$$P_c = P_s + P_b + P_{in} \tag{35}$$

where the time factor $e^{i\omega t}$, common to all force components, has been omitted, and

$$P_s = \int_0^L (k_z + i\omega c_z)\delta_c\, dz = (k_z + i\omega c_z)\delta_c L \tag{36}$$

$$P_b = S_b \delta_c \tag{37}$$

and

$$P_{in} = -mL\omega^2 \delta_c \tag{38}$$

m being the mass per unit length of the pile.

The dynamic stiffness of the pile is finally given by the relationship

$$\mathscr{K}_v = \frac{P_c\, e^{i\omega t}}{\delta_c\, e^{i\omega t}} = S_b + (k_z + i\omega c_z - m\omega^2)L \tag{39}$$

If the pile is subjected to a known δ_c, equation (39) can be used to obtain directly P_c or $\mathscr{K}_v$, once $k_z = k_z(\delta_c)$ and $c_z = c_z(\delta_c)$ have been determined. Iterations, however, will be needed in a force-controlled excitation.

COMPARISONS AND PARAMETRIC RESULTS

Non-linear static response of a pile in Mexico City clay

The method developed here is compared with experimental results from a quasi-static test conducted in Mexico City (Trochanis *et al.*, 1991a,b). In this test a 0·3 m wide, 15 m long, square concrete pile was axially loaded in a clay with undrained shear strength $S_u \approx 40$ kPa, Poisson's ratio $= 0{\cdot}45$ and shear modulus $G_s \approx 6800$ kPa, and with a plasticity index in the region of 200 (typical of the Mexico City clay). Fig. 12 plots the force–displacement relationships from the field test, the proposed method and a non-linear finite element analysis (Zha, 1995). The agreement of the present method with the in situ measurements and the more rigorous analysis is satisfactory.

Distribution of stress/force with depth—comparison with other solutions

The validity of the proposed method is further checked in Figs 13–16 against results from Poulos & Davis (1980). Specifically, Fig. 13 shows that, under elastic conditions, the frequency of the applied load has practically no effect on the distribution with depth of the shear stress on the pile shaft, for an extreme range of E_p/E_s ratios. The agreement with the Poulos & Davis curves is clear in this figure. On the other hand, frequency *does* affect the shear stress distribution and generally plays a more significant role as the applied load increases and non-linear conditions are established; a demonstration is given in Fig. 14 for the case of a medium-intensity load $P_c/P_u = 0{\cdot}25$. In Fig. 15 the distribution with depth of the axial force $N = N(z)$ is shown for different base conditions.

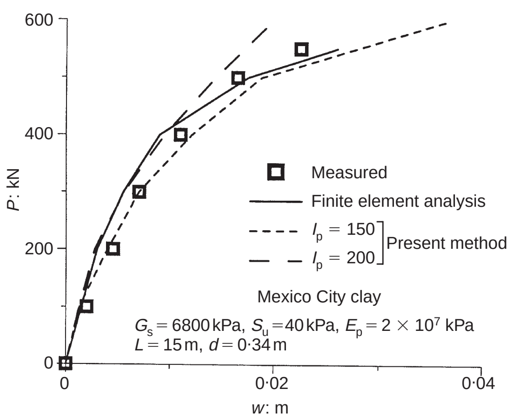

Fig. 12. Verification of the proposed method with real data (full-scale experimental results in Mexico City clay: Trochanis, 1991a,b) and with a more rigorous analysis (finite element analysis results: Zha, 1995)

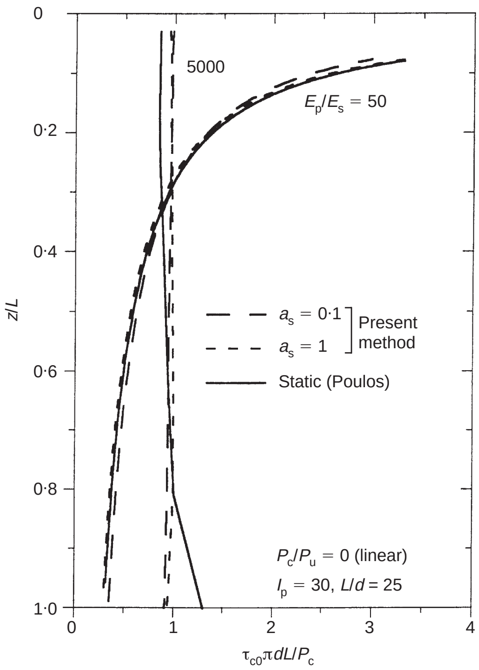

Fig. 13. Distribution of shear stress amplitude along the pile shaft, for two frequencies and two pile–soil stiffness ratios, under elastic conditions

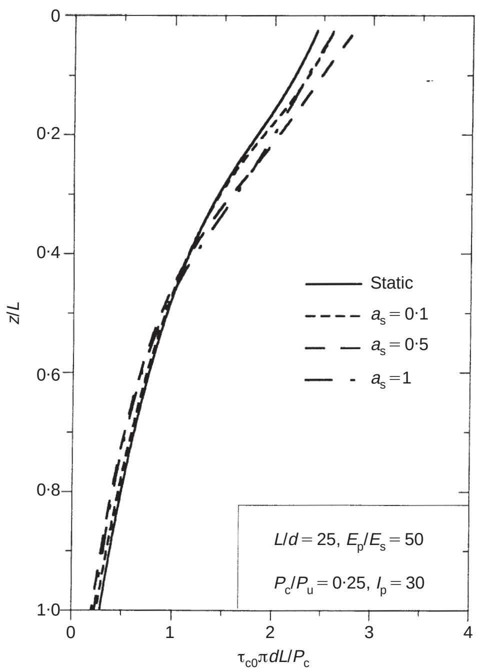

Fig. 14. Distribution of shear stress amplitude along the pile shaft, for static and dynamic conditions, with moderately non-linear soil response ($P_c/P_u = 0{\cdot}25$)

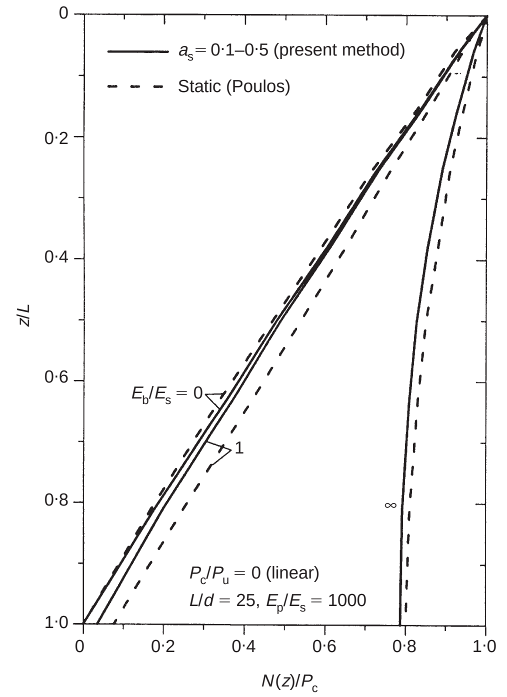

Fig. 15. Distribution of pile axial force with depth, for three different end-bearing conditions, ranging from fixed end ($E_b/E_s = \infty$) to free end ($E_b/E_s = 0$)

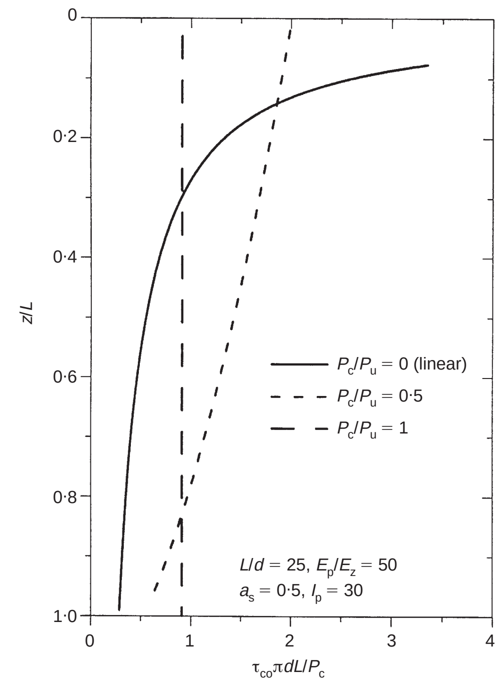

Fig. 16. Distribution of shear stress amplitude along the pile shaft, for three different levels of loading, with soil behaviour ranging from linear to highly non-linear

The force transmitted to the lower part of the pile increases with E_b, the soil modulus of elasticity at the tip level. The good agreement with the curves given by Poulos & Davis (1980) is again evident. On the other hand, Fig. 16 shows that the distribution of shear stresses along the pile shaft becomes increasingly uniform with increasing intensity of the applied load.

Effect of non-linearity on pile-head stiffness and damping

To illustrate the effect of the level of the applied load and the 'plasticity' index of soil on the stiffness and damping of a pile, we consider a concrete pile 0·64 m in diameter and 16 m long, embedded in a homogeneous clay with $E_s = 20$ MPa. Fig. 17 shows, in dimensionless form, the load–displacement curves for $a_s = 0{\cdot}1$ and 0·5. Both real and imaginary parts of the displacement are plotted to illustrate the relative contribution of each component in the resulting displacement. For $a_s = 0{\cdot}1$ (near-static case) the real part (in-phase component) of the response dominates, while the imaginary part (out-of-phase component) becomes significant only at high values of frequency ($a_s =$ 0·5). Notice that the amplitude of the complex

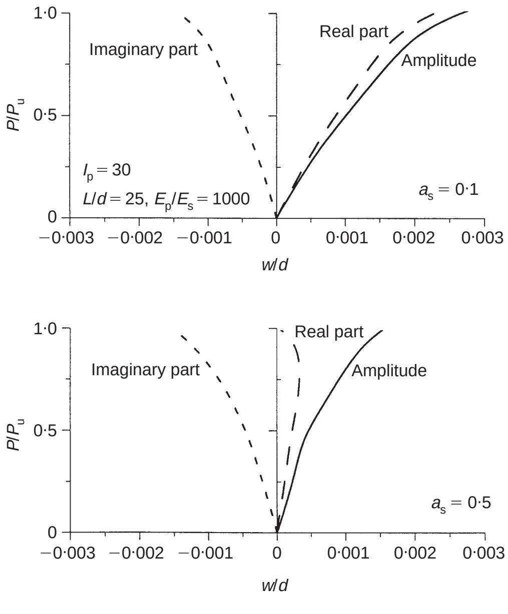

Fig. 17. Load–displacement curves (real part, imaginary part and amplitude) at the head of a pile with $L/d = 25$, $E_p/E_s = 1000$ and $I_p = 30$, for the frequency factors $a_s = 0{\cdot}1$ and $a_s = 0{\cdot}5$

impedance, given by the slope of the 'amplitude' curve, increases with frequency. This is the result of a significant increase in radiation damping.

Figures 18 and 19 illustrate the effect of the magnitude of the applied load and soil 'plasticity' index on the dynamic impedance at the pile head (given in the form $\mathscr{K}_V = K_V + i\omega C_V$). Specifically, Fig. 18(a) plots the variation of pile stiffness as a function of a_s for different values of the level of the applied load; the latter is normalized by P_u, the ultimate static axial load of the pile. The substantial influence of non-linearity on the pile stiffness is obvious for the whole range of frequencies. However, this effect becomes more significant at high values of the frequency factor a_s. On the other hand, the damping ratio plotted in Fig. 18(b) is affected by the level of non-linearity to a generally lesser degree. For large frequencies the value of C_V tends to

$$C_V = 2\pi R L \rho V_s(R) \tag{40}$$

which corresponds to the value of C_V for a pile surrounded by soil with a constant value of S-wave velocity equal to the $V_s(r = R)$ value. In other words, radiation damping decreases in proportion to the decrease in the effective S-wave velocity next to the pile (at $r = R$). This trend is qualitatively similar to the trend observed earlier for the dynamic impedance of the pile *slice* (Figs 6 and 7).

In Fig. 19 the effect of the soil 'plasticity' index is examined for two cases, $I_p = 30$ and $I_p = 100$. It is concluded that with increasing I_p, the soil remains increasingly *elastic* and hence homogeneous for large values of the applied load. It should be noted, however, that for the same shear strength S_u, the soil modulus E_s (or the S-wave velocity at small strains V_s) will be larger as I_p decreases, as, for instance, described by equation (10). As a result, the elastic (linear) stiffness of the soil, and hence of the pile, will be reduced for increasing I_p.

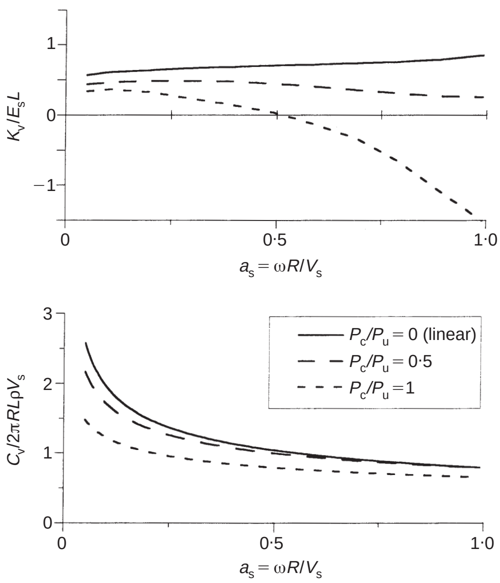

Fig. 18. Effect of level of non-linearity on the dynamic impedance (stiffness and damping) at the head of a pile with $L/d = 25$, $E_p/E_s = 1000$ and $I_p = 30$

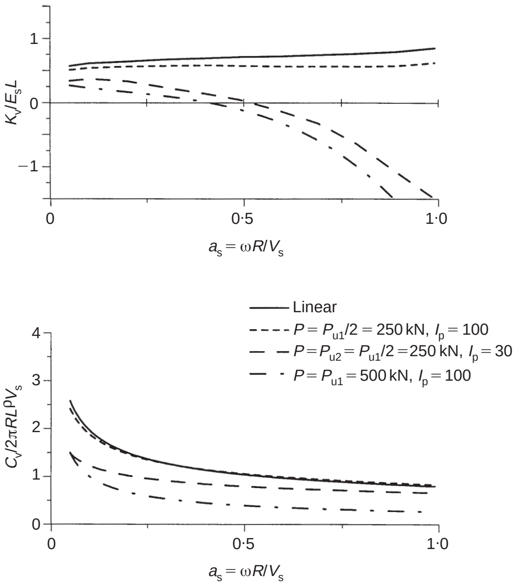

Fig. 19. Dynamic impedance (stiffness and damping) at the head of a pile, with $L/d = 25$ and $E_p/E_s = 1000$ for different types of soil and level of non-linearity

CONCLUSIONS

An axially oscillating pile induces shear strains in the surrounding soil, the amplitude of which attenuates radially away from the pile. In the vicinity of the pile such strains can be large enough to cause non-linear cyclic response of the soil. This paper has developed an equivalent linear method to approximate such a non-linear response. To this end, linear elastic theory has provided amplitudes of shear stresses and shear strains as functions of the radial distance r from the pile. Used in conjunction with published experimental data (in the form of secant shear modulus and damping ratio functions of cyclic strain amplitude and soil 'plasticity' index), the radial distribution of strains was translated into an equivalent shear modulus G, increasing monotonically and continuously with r, from a value of G_0 at the pile–soil interface to the maximum (zero-strain) modulus G_s in the free field, that is, outside the zone of influence of the pile. Thus, a linear but radially inhomogeneous medium replaced the actual non-linear but radially homogeneous soil, allowing analytical derivation of the soil reaction (both the in-phase 'spring' and the out-of-phase 'dashpot' components) against the pile periphery at the particular depth. A simple experimentally motivated approximation was developed to account for slippage at the pile–soil interface. The response of the whole pile could, in general, only be obtained iteratively.

Despite several simplifying approximations, the method seems capable of capturing the key aspects of the non-linear dynamic response. Parametric results have shown that increasing the amplitude of the applied load reduces the stiffness and radiation damping of the system while increasing the hysteretic damping. The significance of non-linearity increases with increasing frequency of pile oscillation, while it decreases with increasing soil 'plasticity' index. On the other hand, frequency has a rather minor effect on the distribution of the axial force along the pile.

It is finally noted that the developed method can utilize experimental data other than those of Vucetic & Dobry (1991) (shear modulus and damping against strain curves) that have been used in this article.

ACKNOWLEDGEMENT

The computer code used for the evaluation of the stiffness of the pile was provided by George Mylonakis, a doctoral student at the State University of New York, Buffalo. The authors modified the code so as to take into account the new impedances found in this study. We are grateful for his help.

APPENDIX 1. SHEAR STRESSES INDUCED IN RADIALLY NON-HOMOGENEOUS ELASTIC MEDIA

It is shown below that the radial distribution of (cyclic) shear stress given in equation (2) is quite *insensitive* to the exact radial variation of shear modulus $G = G(r)$. To this end, the shear modulus is taken to vary as follows:

$$G(r) = G(r_0)\{1 + \mathrm{i}2\xi(R)\}\left(\frac{r}{R}\right)^m \tag{41}$$

For harmonic excitation, the solution of the differential equation of motion (equation (11)) yields

$$w = B_\mathrm{w}\left(\frac{r}{R}\right)^{-m/2} H_\kappa^{(2)}\left(\kappa\lambda_0\left(\frac{r}{R}\right)^{1/\kappa}\right) \tag{42}$$

where B_w is a constant of integration that can be determined from the boundary conditions, $H_\kappa^{(2)}$ is the Hankel function of the second kind of order κ,

$$\kappa = \frac{2}{2-m}$$

$$\lambda_0 = \omega R \frac{\rho}{G(R)[1 + \mathrm{i}2\xi(R)]}$$

and ρ is the mass density.

The shear stress is then given by

$$\tau_\mathrm{c}(r) = G(r)\frac{\mathrm{d}w}{\mathrm{d}r} \tag{43}$$

and the following cases can be investigated, starting with the radially homogeneous case and moving to increasingly inhomogeneous profiles:

Radially homogeneous soil ($m = 0, \xi = 0$) with shear modulus equal to the shear modulus at the pile–soil interface

The radial distribution of shear strength is given by equation (1) and approximately by equation (2).

Soil with shear modulus increasing as the $\frac{2}{3}$ power of r ($m = \frac{2}{3}, \xi = 0$)

The resulting differential equation was solved by Gazetas (1982) for the (mathematically similar) case of a vertically inhomogeneous earth dam, and by Gazetas & Dobry (1984a) for a strip footing. The solution is

$$w = B_\mathrm{w}\sqrt{\left(\frac{4}{3\pi\lambda_0}\right)}\left(\frac{r}{R}\right)^{-2/3} \times \left[\sin\left(\frac{3}{2}\lambda_0\left(\frac{r}{R}\right)^{2/3}\right) + \mathrm{i}\cos\left(\frac{3}{2}\lambda_0\left(\frac{r}{R}\right)^{2/3}\right)\right] \tag{44}$$

from which

$$\frac{\tau_\mathrm{c}(r)}{\tau_\mathrm{c0}} = \left(\frac{r}{R}\right)^{-1/3} \times \sqrt{\left(\frac{a_0^2 + \frac{4}{9}\left(\frac{r}{R}\right)^{-4/3}}{a_0^2 + \frac{4}{9}}\right)} \tag{45}$$

Soil with shear modulus proportional to r ($m = 1, \xi = 0$)

The ratio $\tau_\mathrm{c}(r)/\tau_\mathrm{c0}$ is given by

$$\frac{\tau_\mathrm{c}(r)}{\tau_\mathrm{co}} = \left(\frac{r}{R}\right)^{-1/2}$$

$$\sqrt{\left(\frac{[J_1(t) - a_0\left(\frac{r}{R}\right)^{1/2} J_0(t)]^2 + [Y_1(t) - a_0\left(\frac{r}{R}\right)^{1/2} Y_0(t)]^2}{[J_1(t^*) - a_0 J_0(t^*)]^2 + [Y_1(t^*) - a_0 Y_0(t^*)]^2}\right)} \tag{46}$$

in which

$$t = 2a_0\left(\frac{r}{R}\right)^{1/2} \text{ and } t^* = 2a_0$$

Fig. 20 compares the radial variations of shear stress for the above three cases, $m = 0$, $m = \frac{2}{3}$ and $m = 1$; also plotted is the approximate (asymptotic) equation (2).

The agreement between the two sets of results confirms the insensitivity of the radial variation of shear stress to

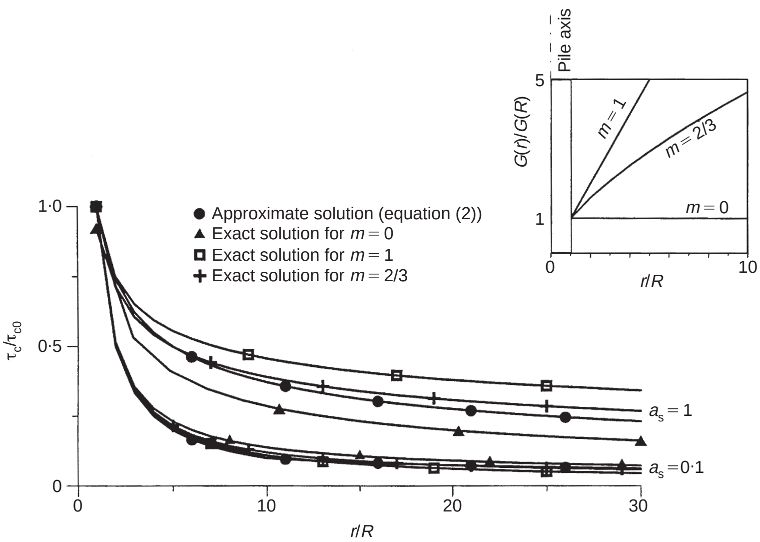

Fig. 20. Variation of shear stress amplitude with radial distance r, for different radial distributions of shear modulus $G = G(r)$, ranging from radially homogeneous ($m = 0$) to strongly inhomogeneous with modulus proportional to r ($m = 1$)

the radial distribution of shear modulus, especially for the most interesting range of low a_0 values ($a_0 < 0{\cdot}5$).

At high frequencies ($a_0 > 0{\cdot}5$) the radial distribution of shear modulus does affect $\tau(r)$. This could be attributed to the fact that for large values of the applied frequency, the short-wavelength waves emitted from the pile 'see' almost only the area next to the pile; as a result, the gradient of $G(r)$ in this area (which varies significantly for the three $G(r)$ functions studied) greatly affects the distribution of $\tau(r)$. For this case, a more accurate approach would be to obtain $\tau_c(r)$ iteratively. Nevertheless, the proposed simplified expression is very close to the most realistic of the three studied distributions, namely the one with $m = \frac{2}{3}$. Therefore in view of the several other approximations of the present method, such iterations are not considered necessary.

NOTATION

a_0	$\omega R/V_{s0}$
A_p	pile cross-sectional area
a_r	$\omega r/V_s(r)$
a_s	$\omega R/V_s$
c_m	$\xi_{es} 2k_s/\omega$ = additional hysteretic dashpot modulus due to slippage
C_v	pile-head dashpot modulus in axial loading (= imaginary part of $\mathscr{K}_v/\omega$)
c_z	'dashpot' modulus
d	pile diameter
E_p	pile modulus of elasticity
F_0	$2\pi R\tau_0(R)$ = static load applied on pile slice (per unit length)
F_c	$2\pi R\tau_{c0}$ = amplitude of cyclic load applied on pile slice (per unit length)
f_s	frictional capacity of soil–pile interface
F_s	$2\pi R f_s$ = yield load of the pile–soil interface (per unit length)
G	$G(r)$ = shear modulus of soil at radial distance r
G_0	shear modulus of soil at $r = R$ (i.e. at the pile–soil interface)
G_s	shear modulus of soil in the far field (i.e. at very low strain levels)
I_p	plasticity index of soil
i	$\sqrt{(-1)}$
k_{imag}	ωc_z = imaginary part of $\mathscr{k}_z$
k_{real}	k_z = real part of $\mathscr{k}_z$
$\mathscr{k}_s$	$k_s + i\omega c_s$ = elasto-plastic complex dynamic impedance accounting for the reduction of spring modulus and radiation damping due to slippage
K_v	pile-head dynamic stiffness modulus in axial loading (= real part of $\mathscr{K}_v$)
$\mathscr{K}_v$	$K_v + i\omega C_v$ = complex pile-head dynamic impedance in axial loading
k_z	'spring' modulus
$\mathscr{k}_z$	$k_z + i\omega c_z$ = complex dynamic impedance of the pile slice
$\mathscr{k}_{zs}$	$k_{zs} + i\omega c_{zs}$ = equivalent elasto-plastic complex dynamic impedance
L	pile length
m	mass of pile per unit length
P_b	force at the pile tip
P_c	amplitude of the sinusoidal applied axial dynamic load
P_{in}	inertial force of the vibrating pile
P_s	total force at the pile shaft
P_U	ultimate axial static load
R	pile radius
r	radial distance from the pile axis

S_b dynamic impedance (stiffness and damping) at the pile base
S_u undrained shear strength of the soil
V_{La} 'Lysmer's analogue' wave velocity
$V_s(r)$ shear wave velocity of soil at radial distance r
V_s shear wave velocity of soil in the far field (i.e. at very low strain levels)
V_{s0} $V_s(R)$ = shear wave velocity of soil at $r = R$ (i.e. at the pile–soil interface)
w $w(r)$ = amplitude of axial displacement of soil at radial distance r
α 'skin friction' parameter ($f_s = \alpha S_u$)
γ_c $\gamma_c(r)$ = amplitude of cyclic shear strain corresponding to $\tau_c(r)$
$\delta(z, t)$ cyclic displacement of pile segment at depth z
δ_0 initial (static) displacement of pile segment
δ_c $\delta_c(z)$ = amplitude of the cyclic displacement of pile segment at depth z. If no slippage occurs $\delta_c = w(R)$
δ_s F_s/k_z = displacement of pile segment required to initiate slippage
Λ loading intensity factor (defined in equation (9))
ξ hysteretic damping factor of soil
ξ_{es} additional hysteretic damping ratio due to slippage
ρ_b mass density of soil below the base of the pile
σ'_{v0} mean effective vertical stress
τ_0 $\tau_0(r)$ = static shear stress on soil element at a radial distance r
τ_c $\tau_c(r)$ = amplitude of cyclic shear stress on soil element at a radial distance r
τ_{c0} $\tau_c(R)$ = amplitude of the imposed cyclic shear stress at the pile–soil interface (if $\tau_{c0} > f_s$ then τ_{c0} is the amplitude of shear stress that would have developed if no slippage occurred)
ω frequency of the applied dynamic load

REFERENCES

Abramowitz, M. & Stegun, I. A. (1972). *Handbook of mathematical functions*. New York: Dover Publications.

Andersen, K. H. (1992). *Foundation design of offshore gravity structures*. Norwegian Geotechnical Institute, Publication No. 185.

Baguelin, F. & Frank, R. (1979). Theoretical studies of piles using the finite-element method. In *Numerical methods in offshore piling*, pp. 83–91. London: Institution of Civil Engineers.

Bouckovalas, G., Gazetas, G. & Stamatelopoulos, S. (1992). Soil parameters for nonlinear analysis of axial pile vibration. *Proc. 2nd Hellenic Conf. on Geotechnical Engng, Thessaloniki*, Vol. 2, pp. 467–477.

Burland, J. B. (1989). 9th Bjerrum Memorial Lecture: Small is beautiful—the stiffness of soils at small strains. *Can. Geotech. J.* **26**, 499–516.

Chrysikou, E. (1993). *Nonlinear dynamic analysis of axial pile vibration.* Diploma Thesis, Geotechnical Department, Athens: National Technical University.

Dobry, R. & Gazetas, G. (1988). Simple method for dynamic stiffness and damping of floating pile groups. *Géotechnique* **38**, No. 4, 557–574.

Dobry, R. & Vucetic, M. (1987). State of the art report: Dynamic properties and response of soft clays deposits. *Proc. Int. Symp. on Geotechnical Engineering of Soft Soils* **2**, 51–87.

Dotson, K. W. & Veletsos, A. S. (1990). Vertical and torsional impedances for radially inhomogeneous viscoelastic soil layers. *Soil Dyn. Earthq. Engng* **9**, No. 3, 110–119.

Fleming, W. G. K., Weltman, A. J., Randolph, M. F. & Elson, W. K. (1985). *Piling engineering*. Surrey University Press.

Gazetas, G. (1982). Shear vibrations of vertically inhomogeneous earth dams. *Int. J. Num. Anal. Meth. Geomech.* **6**, No. 1, 219–241.

Gazetas, G. (1983). Analysis of machine foundation vibrations: state of the art. *Soil Dyn. Earthq. Engng* **2**, No. 1, 2–43.

Gazetas, G. & Dobry, R. (1984a). Simple radiation damping model for piles and footings. *Journal of Engineering Mechanics*, ASCE 110, No. 6, 937–956.

Gazetas, G. & Dobry, R. (1984b). Horizontal response of piles in layered soils. *J. Geotech. Engng*, *ASCE* **110**, No. 1, 20–40.

Gazetas, G. & Makris, N. (1991). Dynamic pile-soil-pile interaction. Part I: Analysis of axial vibration. *Earthq. Engng Struct. Dyn.* **20**, No. 2, 115–132.

Gibson, R. E. (1967). Some results concerning displacements and stresses in a non-homogeneous elastic halfspace. *Géotechnique* **17**, No. 1, 58–67.

Gibson, R. E. (1968). Correspondence on: Some results concerning displacements and stresses in a non-homogeneous elastic halfspace. *Géotechnique* **18**, No. 2, 275–276.

Gibson, R. E. (1974). The analytical method in soil mechanics. *Géotechnique* **24**, No. 2, 115–140.

Gibson, R. E. & Sills, G. C. (1972). Some results concerning the plane deformation of a non-homogeneous elastic half space. *Stress–strain behaviour of soils, Proc. Roscoe Memorial Symposium* (ed. R. H. Parry), pp. 564–572.

Jardine, R. J., Symes, M. J. & Burland, J. B. (1984). The measurement of soil stiffness in the triaxial apparatus. *Géotechnique* **34**, No. 3, 323–340.

Kraft, L., Ray, R. & Kagawa, T. (1981). Theoretical *t–z* curves. *J. Geotech. Engng Div.*, *ASCE* **107**, No. GT11, 1543–1562.

Kuwabara, F. (1991). Settlement behaviour of non-linear soil around single piles subjected to vertical loads. *Soils and Foundations* **31**, No. 1, 39–46.

Larsson, R. & Mulabdic, M. (1991). *Shear moduli in Scandinavian clays*. Swedish Geotechnical Institute, Publication No. 40.

Makris, N. & Gazetas, G. (1993). Displacement phase differences in a harmonically oscillating pile. *Géotechnique* **43**, No. 1, 135–150.

Masing, G. (1926). Eigenspannumyen und Verfeshungung beim Messing. *Proc. Int. Congress for Applied Mechanics*, pp. 332–335.

Michaelides, O. & Gazetas, G. (1995). Impedance function of piles in inhomogeneous media. *J. Geotech. Engng, ASCE* **121**, No. 2, 234–236.

Morse, P. M. & Ingard, K. U. (1968). *Theoretical acoustics*. New York: McGraw-Hill.

Novak, M. (1974). Dynamic stiffness and damping of piles. *Can. Geotech. J.* **11**, No. 4, 574–598.

Novak, M., Nogami, T. & Aboul-Ella, F. (1978).

Dynamic soil reactions for plane-strain case. *J. Engng Mech.*, *ASCE* **104**, No. 4, 953–959.
Novak, M. (1991). Piles under dynamic loads. *Proc. 2nd Int. Conf. on Recent Advances in Geotechnical Earthquake Engineering and Soil Dynamics, St. Louis*, Vol. 3, pp. 2433–2456.
Novak, M. & Sheta, M. (1980). Approximate approach to contact effects of piles. In *Special technical publication on dynamic response of pile foundations: analytical aspects* (eds M. W. O'Neill & R. Dobry). New York: ASCE.
Pender, M. J. (1993). Aseismic pile foundation design analysis. *Bull. New Zealand National Soc. for Earthq. Engng* **26**, No. 1, 49–161.
Poulos, H. G. & Davis, E. H. (1980). *Pile foundation analysis and design*. New York: Wiley.
Poulos, H. G. (1988). *Marine geotechnics*. London: Unwin Hyman.
Randolph, M. F. & Wroth, C. P. (1978). Analysis of deformation of vertically loaded piles. *J. Geotech. Engng Div.*, *ASCE* **104**, No. GT12, 1465–1488.
Richart, F. E. & Wylie, E. B. (1977). Influence of dynamic soil properties on response of soil masses. In *Structural and geotechnical mechanics* (ed. W. J. Hall). New York: Prentice-Hall.
Scott, R. F. (1981). *Foundation analysis*. New York: Prentice-Hall.
Seed, H. B. & Idriss, I. M. (1970). *Soil moduli and damping factors for dynamic response analyses*. Report No. EERC 70-10, University of California, Berkeley.
Spiegel, M. R. (1971). *Theory and problems of advanced mathematics for engineers and scientists. Schaum's Outline Series*, New York: McGraw-Hill.
Tomlinson, M. J. (1986). *Foundation design and construction*, 5th edition. London: Longman.
Trochanis, A. M., Bielak, J. & Christiano, P. (1991a). Three-dimensional nonlinear study of piles. *J. Geotech. Engng Div., ASCE* **117**, No. 2, 429–447.
Trochanis, A. M., Bielak, J. & Christiano, P. (1991b). Simplified model for analysis of one or two piles. *J. Geotech. Engng Div., ASCE* **117**, No. 2, 448–466.
Veletsos, A. S. & Dotson, K. W. (1986). Impedances of soil layer with disturbed boundary zone. *J. Geotech. Engng Div., ASCE* **112**, No. 3, 363–368.
Veletsos, A. S. & Dotson, K. W. (1988). Vertical and torsional vibration of foundations in inhomogeneous media. *J. Geotechnical Engineering Division*, ASCE **114**, No. 9, 1002–1021.
Viggiani, G. & Atkinson, J. H. (1995). Stiffness of fine-grained soil at very small strains. *Géotechnique* **45**, No. 2, 249–265.
Vucetic, M. & Dobry, R. (1991). Effect of soil plasticity on cyclic response. *J. Geotech. Engng, ASCE* **117**, No. 1, 89–107.
Zha, J. (1995). *Finite element analysis of nonlinear dynamic pile–soil interaction*. PhD thesis, New York State University at Buffalo.